

Berry-Phase Translation of X Rays by a Deformed Crystal

Yoshiki Kohmura, Kei Sawada, and Tetsuya Ishikawa

RIKEN, SPring-8 Center, 1-1-1, Kouto, Sayo-cho, Sayo-gun, Hyogo 679-5148, Japan

(Received 21 December 2009; published 14 June 2010)

We experimentally demonstrated an enhanced translation of an x-ray beam nearly parallel to the diffracting planes over millimeter distances in a deformed silicon crystal. This effect is a consequence of the Berry-phase effect in phase space [K. Sawada *et al.*, *Phys. Rev. Lett.* **96**, 154802 (2006)], which enables an interplay between the gap in the dispersion surface in momentum space and the atomic displacements in real space. Such an interplay in phase space enhances the beam translation by some 5 orders of magnitude, leading to the macroscopic effect.

DOI: 10.1103/PhysRevLett.104.244801

PACS numbers: 41.50.+h, 42.25.Bs, 42.25.Fx

Refraction phenomena are the basis of most optics in the visible region of the spectrum. An x-ray beam, however, has very weak interaction with matter that gives a tiny refraction, which scales as λ^2 , where λ is the wavelength. Therefore, x-ray optics often uses diffraction to control the x-ray beam, and for many optical elements a high degree of crystal perfection is desirable and necessary. Here we demonstrate a new optical effect for x rays [1] that allows enhanced translation of an x-ray beam nearly parallel to the diffraction planes. This effect reveals a new aspect of the Berry phase [2] associated with two ingredients—a nearby Bragg reflection and, unusually, a strain field in the crystal. The combination of the two together allows a shift in the x-ray beam that scales as $1/\lambda^2$, leading to macroscopic changes in the x-ray propagation.

In a perfect crystal, x-ray wave packet propagation is described by the group velocity, $\vec{v}_{\text{perfect}} = \vec{\nabla}_k \omega(\vec{k})$, where $\omega(\vec{k})$ is a frequency and \vec{k} is a wave vector. This group velocity is normal to the dispersion surface in momentum space [Fig. 1(a)] and does not depend on position. However, when the crystal has a deformation in real space given as $\vec{r} \rightarrow \vec{r} + \vec{u}(\vec{r})$ as shown in Fig. 1(b), the propagating direction should have a position dependence, and requires some correction to the group velocity. This correction is a consequence of a coupling between real and momentum spaces, introducing a Berry-phase term to the beam trajectory given as [1]

$$\vec{r}_c(t) = \vec{v}_{\text{perfect}} t + \vec{G} \left[\frac{1}{2k^2} \vec{G} \cdot \vec{u}(\vec{r}_c) \right] \frac{k}{\Delta k}, \quad (1)$$

where \vec{r}_c is the center position of a wave packet near the Bragg condition, t is time, \vec{G} is a reciprocal-lattice vector, $k \equiv |\vec{k}|$, and Δk is a gap in momentum space [Fig. 1(a)]. The first term on the right-hand side is the group velocity term independent of position, and gives the Borrmann fan effect [3] or Bragg-Laue diffraction [4]. The second term is the focus of this Letter. This term represents a correction to the group velocity that gives a position dependence due to the deformation. This correction term is known as the

Berry-phase effect [2] associated with an interplay between the deformation in real space and the gapped dispersion in momentum space [1]. Because of the correction term, the beam velocity is shifted from \vec{v}_{perfect} towards the \vec{G} direction. This shift is a factor $k/\Delta k \sim 10^5$ – 10^6 larger than the atomic displacement \vec{u} and scales as $1/\lambda^2$. This factor makes the beam translation macroscopic. It is worth noting that the beam translation does not introduce any change in the wave vector \vec{k} . In this sense, this effect is distinct from refraction.

Figure 2(a) is a schematic of the effect. The incident x-ray beam receives a millimeter-scale translation inside the crystal due to a nanometer-scale deformation, and reaches the edge. During this translation, the beam has negligible change of its wave vector, which gives negligible refraction. The deformed region of the crystal guides the x-ray beam, but, in strong contrast to reflection-based waveguides, does not introduce any beam divergence. Figure 2(b) is a schematic diagram of the designed crystal

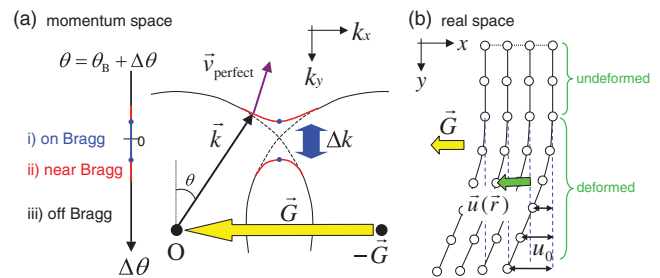


FIG. 1 (color). (a) Dispersion curves in a two-dimensional momentum space with a gap Δk at the Bragg condition. The two curved lines are constant-frequency contours on the 2D dispersion surface $\omega(\vec{k})$. They represent the allowed propagating modes of x rays with $\omega(\vec{k}) = \text{const}$ inside a perfect crystal. The offset angle $\Delta\theta$ from the Bragg angle θ_B satisfies $\Delta\theta/\theta_B \approx \Delta k/|k|$ for near-Bragg conditions. (b) Crystal deformation in real space with an atomic displacement $\vec{r} \rightarrow \vec{r} + \vec{u}(\vec{r})$. Dashed lines represent crystal planes for a perfect crystal. u_0 is an amount of atomic displacement at the bottom surface layer.

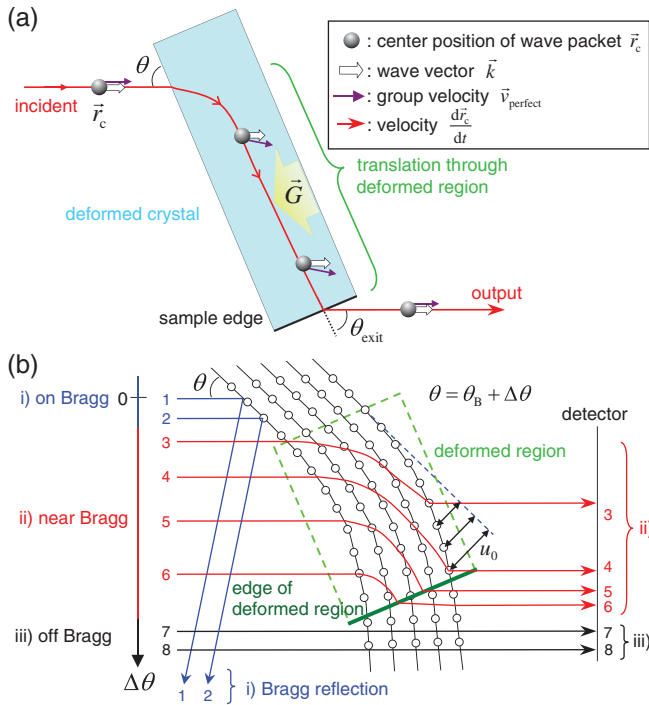


FIG. 2 (color). (a) Schematic illustration of the discovered phenomena. The beam exhibits a translation inside the deformed region, reaches the sample edge, and exits without angular divergence. (b) Schematic diagram of the designed crystal curved to observe the phenomena. The incident x rays are composed of several wave packets that experience three distinct varieties of propagation (i)–(iii), depending on the incident angle. (i) On-Bragg condition, the total reflection occurs (paths 1 and 2). (ii) Near-Bragg condition, the enhanced beam translation occurs (paths 3–6). At the edge of the deformed region, the exit beam travels parallel to the incident one and forms a peak at the detector (paths 5 and 6). (iii) Far beyond the Bragg condition, the beams propagate through the crystal without any large beam translation (paths 7 and 8).

curved to observe the phenomena. The experimental x-ray beam is composed of a set of several wave packets. Each wave packet has a different wave vector and a trajectory described by Eq. (1). Thus, we can identify three different regions of behavior (i)–(iii) depending on the deviation $\Delta\theta$ of each wave packet from the Bragg angle θ_B (see caption for details). The macroscopic translation occurs when the diffracting crystal plane of the deformed region of the crystal is set near the Bragg condition. This effect collects the paths to the edge of the deformed region, resulting in a sharp peak at the detector.

In an experiment, we used a silicon crystal with the thickness of 100 μm . Its surface was oxidized to introduce microscopic deformation. The deformation was spread over the entire crystal by using the wax that fixes the crystal on a holder as in Fig. 3(a). The amount of the deformation was adjusted to be larger than $u_0^{\text{min}} = 80 \text{ nm}$, which is theoretically required to give an x-ray translation of 5 mm [5] so that a beam reaches the edge of the sample

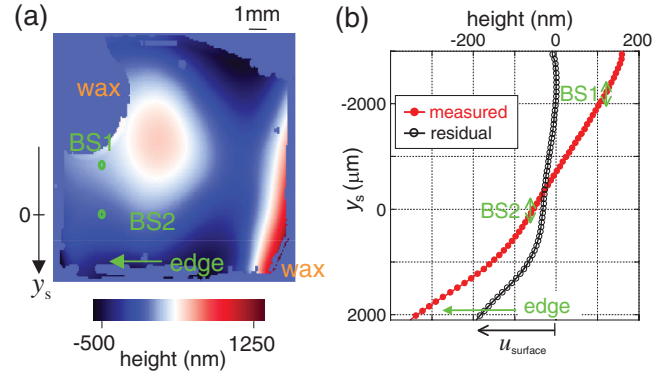


FIG. 3 (color). (a) Surface profile of the sample crystal, 14 mm \times 11 mm, measured with a Fizeau interferometer GPI XPHR by Zygo Corp. The green ovals show the size (FWHM) and the location of the illuminating beam spots (BS). The concave surface was set to the incident beam. (b) Vertical profile of (a) along y_s direction passing through the BSs with the residual from a linear function, where y_s is a position coordinate on the sample surface.

as shown in Fig. 2(a). In Fig. 3(a), the surface-height distribution, measured by a visible-light interferometer, is represented. We chose two x-ray illuminating beam spots (BS) in Fig. 3(a) in order to measure the positional dependence of the Berry-phase effect, as shown later. The surface-height profile along these BSs are shown in Fig. 3(b), together with the residual from a linear function which corresponds to the deformation at the crystal surface. The amount of the deformation at the top surface layer measured from BS1 (BS2) to the edge of the crystal was $u_{\text{surface}} = 190$ (160) nm [Fig. 3(b)]. A relation between u_{surface} and the deformation inside the crystal is examined by using x rays.

We used a 15 keV x-ray beam at the SPring-8 undulator beam line BL19LXU [6]. The experimental setup is shown in Fig. 4. The incident angle onto the sample crystal was set near the Bragg angle $\theta_B = 17.6^\circ$ for the silicon (400) plane. From the rocking curve measurements, the Darwin width was approximately 4 arcsec (FWHM) for both BSs, and was much broadened from the intrinsic width, 1.6 arcsec, due to the deformation. This broadening implies that atomic displacements inside the crystal are of the same orders of magnitude as those at the top surface u_{surface} and that at the bottom layer u_0 .

In Fig. 5, experimental results for s polarization are represented. In Fig. 5(a), the entire x-ray beam was far from the Bragg condition, offset by 30 arcsec, and was transmitted without any shift. In Figs. 5(b) and 5(c), some wave packets in a beam are at the Bragg condition, and are totally reflected, corresponding to paths 1 and 2 in Fig. 2(b). This Bragg reflection separates the transmitted beam into two islands and is observed as the dark regions at the left half of the beam in Figs. 5(b) and 5(c), indicated by arrows. Note that the slant shape of the dark regions represents the two-dimensional distribution of the bend [see Fig. 3(a)].

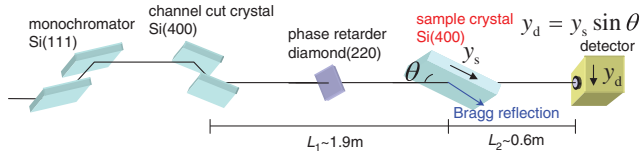


FIG. 4 (color). Experimental setup. The channel cut and the monochromator crystals were set in $(++)$ arrangement to reduce the energy bandwidth and the angular divergence of the output beam. A phosphor-coupled x-ray camera with $4.55 \mu\text{m}$ effective pixel size was used as a detector. The Bragg reflection was also confirmed by an independent counter in the θ - 2θ reflection geometry. The coordinate $y_d \equiv y_s \sin \theta$ represents a position on the detector. The polarization state of the beam was switched from s polarization to p polarization by using a diamond crystal phase retarder with the thickness of 2 mm.

To analyze the Berry-phase effect occurring at the near-Bragg condition, the narrow green window was chosen next to the dark regions. In this window, we observed bright peaks at large y_d due to the expected beam translation. Figure 5(d) shows the vertical intensity profiles for Figs. 5(a)–5(c). We found the translated peak moved at the detector by the same amount as the crystal movement [see caption of Fig. 5(d)]. This is caused by the expected x-ray

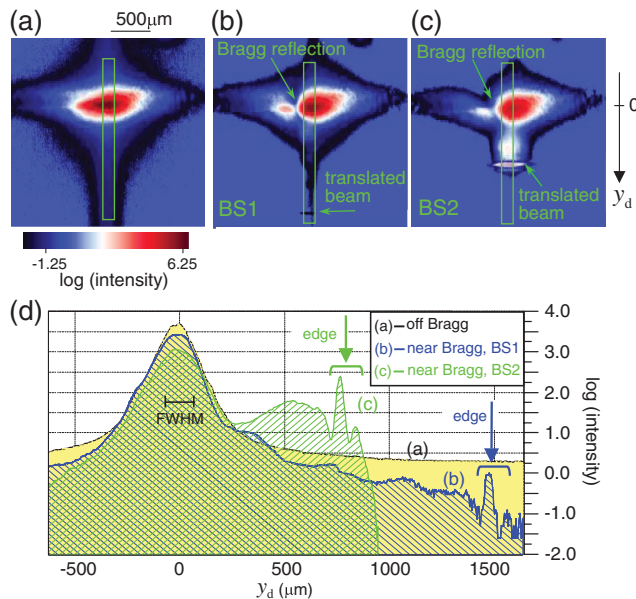


FIG. 5 (color). Intensity distributions of the crystal transmitted image in a common logarithmic scale with (a) off-Bragg condition and (b),(c) near-Bragg condition on two different beam spots BS1 and BS2, respectively. The crystal was set to be $700 \mu\text{m}$ higher in the case of (c) than in (b). The sharp peaks due to the enhanced translation were observed in the two images indicated by arrows. (d) Vertical intensity projection analyzed from the images in (a)–(c). The displacement of the peaks with arrows in (b) for BS1 and in (c) for BS2, from $y_d = 1500$ to $800 \mu\text{m}$ away from the beam center, coincided with the crystal movement of $700 \mu\text{m}$.

beam translation and its termination at the crystal edge, corresponding to Fig. 2(a). It implies a waveguiding effect of the wave packet traveling through the crystal with the peak position shift of 1.5 mm at the detector, corresponding to a path length of about 5 mm within the crystal. This translation is some 5 orders of magnitude larger than an atomic displacement u_0 [Fig. 1(b)], and is caused by the bend in the entire crystal.

The translation of the beam does not introduce angular divergence. The sharp peaks, e.g., at $y_d = 1500 \mu\text{m}$ for the BS1 near the Bragg condition [line b in Fig. 5(d)], imply an extremely low exit angular divergence as follows: the observed width of the line peak, $40 \mu\text{m}$ (FWHM), and the distance between the crystal and the x-ray imaging sensor, $L_2 \approx 0.6 \text{ m}$ (Fig. 4), give an upper limit of 14 arcsec for the exit angular divergence. This is 2 orders of magnitude smaller than the typical critical angle for total reflection in a heavy metal x-ray waveguide.

The observed phenomena cannot be explained by refraction, but by translation of the x rays for the following reasons. First, a large deflection angle at the incident surface of 16.4° was observed [7]. The refraction angle at the surface should be less than 1.4 arcsec , and refraction never gives such a large deflection angle. Second, an exit angle, $\theta_{\text{exit}} \approx \theta$ ($\approx 17.6^\circ$) [see Fig. 2(a)], was much larger than that expected from the normal refraction, 1.2° [7]. Third, the exit beam is parallel to the incident beam. These strongly suggest that the observed trajectories are due to the translation of x rays rather than to their normal refraction.

Moreover, an apparent change of the intensity distribution of the translated x rays was observed by comparing the cases of both BSs in Fig. 5(d). A significantly broad peak at $y_d = 600 \mu\text{m}$ was observed only in the case of BS2 and not in BS1. This is clear evidence of the x-ray translation depending on the x-ray incident position and the strain field [as in Figs. 3(a) and 3(b)], strongly supporting the new optical effect [1]. Note that the change of the translated distance and x-ray attenuation inside the crystal do not affect the intensity profile in this manner.

The Berry-phase x-ray translation effect is sensitive to a small variation of the strain field due to the oxidation, as we show in the following example where one edge of the deformed region was visualized as schematically shown in Fig. 6(a). We analyzed this effect by measuring the angle dependence at a different spot from BSs 1 and 2. Shown in Fig. 6(b) is the vertical intensity projections of the transmitted images for three different glazing incidence angles $\Delta\theta$, as a function of position on the detector. Near the Bragg condition ($\Delta\theta = -2 \text{ arcsec}$), the overall transmitted intensity is reduced from those at the other two angles due to the Bragg reflection. Remarkably, a sharp peak around $y_d = 490 \mu\text{m}$ was observed at $\Delta\theta = -2 \text{ arcsec}$ (near the Bragg reflection), and vanished completely at larger offset angles (off the Bragg reflection).

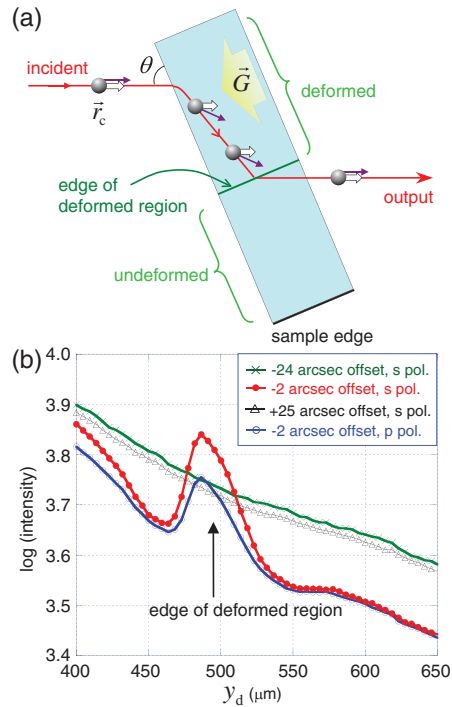


FIG. 6 (color). (a) Schematic illustration of the beam exiting at the edge of deformed region. (b) Vertical intensity projections of the transmitted images, for three different glazing incidence angles with s -polarized x rays, and for one angle with p -polarized x rays, on a common logarithmic scale. The peak was clearly observed only at the incident angles of -2 arcsec, not at large offset angles of -24 and $+25$ arcsec. The peak intensity was 1.4 times higher with s -polarized x rays than with p -polarized x rays, consistent with the Darwin width ratio.

Measurement of the polarization dependence clarified the origin of this sharp peak. The Darwin width for p polarization is smaller than that for s polarization and a larger amount of translation was expected from Eq. (1). However, the observed peak position did not depend on the polarizations as shown in Fig. 6(b) and suggested a fixed edge of the deformed region as in Fig. 6(a). A lower peak intensity was observed for p polarization than that for s polarization due to the smaller Darwin width.

The Berry-phase translation of an x-ray beam will open a door to the new optical research based on the x-ray Berry phase, as the Berry-phase effects on wave packet propagation in various systems [8–12] have been of much interest. Since the x-ray beam-translation effect is related to the deformed crystal plane, it potentially can be used for waveguides by carefully designing crystals. Furthermore, the diagnosis of deformed crystals is possible, even more effectively by measuring the distribution of the translation

with spatially confined incident beams. Ultrafast diagnosis, such as with a subpicosecond time resolution, could be realized using the advent of extremely intense short pulse x-ray sources such as the free electron laser [13–15]. Note that the low angular divergence of the exit beam enables all these measurements at arbitrary camera distances, unlike the case for conventional x-ray waveguides [16,17].

The authors are grateful to Y. Teraoka, M. Suzuki, A. Kishida, H. Ohsumi, and T. Komesu for experimental assistance, and to A. Baron, M. Yabashi, M. Saito, S. Murakami, and N. Nagaosa for fruitful discussions. This work is supported by KAKENHI (21340086 and 20340081) from JSPS of Japan.

- [1] K. Sawada, S. Murakami, and N. Nagaosa, *Phys. Rev. Lett.* **96**, 154802 (2006).
- [2] M. V. Berry, *Proc. R. Soc. A* **392**, 45 (1984).
- [3] G. Borrmann and H. Wagner, *Naturwissenschaften* **42**, 68 (1955).
- [4] H. Wagner, *Z. Phys.* **146**, 127 (1956).
- [5] Using the distance between the BS1 and the sample edge, 5 mm, and Eq. (1), we obtain the amount of deformation to be $u_0^{\min} = 5 \text{ mm} \times (2\Delta k/k) \tan\theta_B \approx 80 \text{ nm}$, assuming that the intrinsic gap is $\Delta k/k \approx 2.5 \times 10^{-5}$.
- [6] M. Yabashi, T. Mochizuki, H. Yamazaki, S. Goto, H. Ohashi, K. Takeshita, T. Ohata, T. Matsushita, K. Tamasaku, Y. Tanaka, and T. Ishikawa, *Nucl. Instrum. Methods Phys. Res., Sect. A* **467**, 678 (2001).
- [7] The deflection angle is calculated by $\theta_B - \theta_0 = 16.4^\circ$, where $\theta_0 = 1.2^\circ$ is an angle between the surface and a line connecting BS1 and an exit spot for 5 mm path length and 0.1 mm thickness of the crystal.
- [8] Y. Zhang, Y.-W. Tan, H. L. Stormer, and P. Kim, *Nature (London)* **438**, 201 (2005).
- [9] P. J. Leek, J. M. Fink, A. Blais, R. Bianchetti, M. Goppl, J. M. Gambetta, D. I. Schuster, L. Frunzio, R. J. Schoelkopf, and A. Wallraff, *Science* **318**, 1889 (2007).
- [10] F. D. M. Haldane and S. Raghu, *Phys. Rev. Lett.* **100**, 013904 (2008).
- [11] M. Onoda, S. Murakami, and N. Nagaosa, *Phys. Rev. Lett.* **93**, 083901 (2004).
- [12] O. Hosten and P. Kwiat, *Science* **319**, 787 (2008).
- [13] J. Arthur *et al.*, SLAC Report No. SLAC-R593, 2002.
- [14] “SCSS X-FEL Conceptual Design Report,” edited by T. Tanaka and T. Shintake, RIKEN Harima Institute, 2005.
- [15] *XFEL: The European X-Ray Free-Electron Laser*, Technical Design Report, edited by M. Altarelli *et al.*, DESY, 2006.
- [16] D. H. Bilderback, S. A. Hoffman, and D. J. Thiel, *Science* **263**, 201 (1994).
- [17] F. Pfeiffer, C. David, M. Burghammer, C. Riekel, and T. Salditt, *Science* **297**, 230 (2002).